Order-disorder transition in a two-dimensional associating lattice gas

A. P. Furlan [1,*] Tiago J. Oliveira,[2] Jürgen F. Stilck,[3] and Ronald Dickman[4]

[1]*Departamento de Física, ICEx, Universidade Federal de Minas Gerais, C. P. 702, 30123-970 Belo Horizonte, Minas Gerais, Brazil*
[2]*Departamento de Física, Universidade Federal de Viçosa, 36570-900, Viçosa, Minas Gerais, Brazil*
[3]*Instituto de Física and National Institute of Science and Technology for Complex Systems,*
Universidade Federal Fluminense, Niterói, Rio de Janeiro, Brazil
[4]*Departamento de Física and National Institute of Science and Technology for Complex Systems, ICEx,*
Universidade Federal de Minas Gerais, C. P. 702, 30123-970 Belo Horizonte, Minas Gerais, Brazil

We study an associating lattice gas (ALG) using Monte Carlo simulation on the triangular lattice and semianalytical solutions on Husimi lattices. In this model, the molecules have an orientational degree of freedom and the interactions depend on the relative orientations of nearest-neighbor molecules, mimicking the formation of hydrogen bonds. We focus on the transition between the high-density liquid (HDL) phase and the isotropic phase in the limit of full occupancy, corresponding to chemical potential $\mu \to \infty$, which has not yet been studied systematically. Simulations yield a continuous phase transition at $\tau_c = k_B T_c / \gamma = 0.4763(1)$ (where $-\gamma$ is the bond energy) between the low-temperature HDL phase, with a nonvanishing mean orientation of the molecules, and the high-temperature isotropic phase. Results for critical exponents and the Binder cumulant indicate that the transition belongs to the three-state Potts model universality class, even though the ALG Hamiltonian does not have the full permutation symmetry of the Potts model. In contrast with simulation, the Husimi lattice analyses furnish a discontinuous phase transition, characterized by a discontinuity of the nematic order parameter. The transition temperatures ($\tau_c = 0.51403$ and 0.51207 for trees built with triangles and hexagons, respectively) are slightly higher than that found via simulation. Since the Husimi lattice studies show that the ALG phase diagram features a discontinuous isotropic-HDL line for finite μ, three possible scenarios arise for the triangular lattice. The first is that in the limit $\mu \to \infty$ the first-order line ends in a critical point; the second is a change in the nature of the transition at some finite chemical potential; the third is that the entire line is one of continuous phase transitions. Results from other ALG models and the fact that mean-field approximations show a discontinuous phase transition for the three-state Potts model (known to possess a continuous transition) lends some weight to the third alternative.

I. INTRODUCTION

It is no news that water exhibits quite unusual thermodynamic behavior, characterized by a set of anomalies, among which the anomaly in density is the best known [1]. In recent decades, many models were developed with the purpose of investigating the fundamental mechanisms which lead to the water anomalies. Among them, lattice models have attracted much attention due to their easy implementation and low computational cost. These models usually include soft-core potentials to represent excluded volume effects, and orientational interactions to represent hydrogen bonding between molecules. So far, these models are only able to reproduce some of the anomalies qualitatively. Despite this, they exhibit rich phase diagrams that provide an ideal environment for the study of phase transitions as well as the validation of new computational techniques.

The first orientational lattice model for water, proposed by Bell and Lavis (BL) [2–4], is defined on a triangular lattice in which each site can be either vacant or occupied by a molecule. The molecules possess three bonding directions with $120°$ between them, resulting in two orientational states per molecule. The model exhibits three phases: gas, low density liquid (LDL) and high-density liquid (HDL) [5] at low, intermediate and high chemical potentials, respectively. While the gas-LDL transition is known to be discontinuous, characterized by a jump in density, the nature of the liquid-liquid transition is still controversial. For example, mean-field approximations (Bethe lattice solutions [6] and cluster-variation methods [7]) point to a discontinuous phase transition, whereas Monte Carlo (MC) simulations [5,8] show a continuous transition. There is no consensus regarding the universality class of this transition. Fiore *et al.* [5] assert that it falls into the Ising universality class, while Šimėnas *et al.* [8] report three-state Potts critical exponents.

Following the ideas of Bell and Lavis, Henriques and Barbosa introduced a two-dimensional (2D) associating lattice gas (ALG) [9]. In this model, also defined on a triangular lattice, each molecule has four bonding arms and two inert ones, the latter taking opposite directions on the lattice. Two of the bonding arms are proton donors in hydrogen bonds, while two are receptors, leading to 18 states per molecule. The model [9] also exhibits gas, LDL, and HDL phases, but in

*apfurlan@fisica.ufmg.br

contrast to simulation results for the BL model, the LDL and HDL phases are separated by a discontinuous transition line that ends at a bicritical point. There is also a gas-HDL line of continuous transitions, which starts at the bicritical point and seems to extend to large values of the chemical potential. The LDL and gas phases are separated by a continuous and a discontinuous transition line, which connect at a tricritical point. The former line meets the LDL-HDL and gas-HDL lines at the bicritical point [10].

Variants of the ALG model have been investigated, among them, three-dimensional (3D) [11–13] and symmetric versions [14,15]. The 3D model [11,12] is defined on a body-centered cubic lattice in which each molecule possesses four bonding and four inert arms. Despite the differences in geometry and number of orientational states in relation to the original ALG model [9], the three-phase (gas, LDL, HDL) behavior is preserved. While a phase diagram featuring two tricritical points was suggested by Buzanno *et al.* [16] based on a cluster-variation approach, simulation results by Szortyka *et al.* [12] indicate that there is in fact a tricritical and a bicritical point, similar to the 2D case [10]. In the 3D model, however, a gas-LDL coexistence line meets the continuous LDL-HDL and gas-HDL transition lines at the bicritical point [12].

The symmetric ALG model makes no distinction between donor and receptor bonding arms. This leads to a simplification, since the number of states per particle is substantially reduced. Balladares *et al.* [14] investigated this model on the triangular lattice and found only two discontinuous (gas-LDL and a LDL-HDL) transition lines in the phase diagram, each ending at a critical point. As an aside, let us remark that this very same scenario was reported in the former studies of the original 2D ALG model [9] and of the 3D version [11]. It turns out that they were incorrect, as demonstrated in more recent analyses [10,12,16], as discussed above. In fact, the semianalytical solution of the symmetric model [14] on a Husimi lattice build with hexagons (which is a mean-field approximation for the triangular lattice) unveils a phase diagram with three coexistence lines (gas-LDL, gas-HDL and LDL-HDL) meeting at a triple point [17]. Moreover, more recent simulations of this model have provided evidence that the critical points reported in Ref. [14] are actually tricritical points [15], so that the thermodynamic behavior of this model is closer to that of the other versions. In contrast with these cases and with the mean-field results, however, a gas-HDL transition has not yet been observed in simulations of the 2D symmetric ALG, so that the existence of a continuous order-disorder transition and its universality class remains unclear for this model. In fact, studies of the critical exponents at the continuous phase transitions of all versions of the ALG model are still lacking.

Motivated by this issue, we study the phase transition in the full-occupancy limit of the symmetric 2D ALG model [14], using MC simulations (employing both Wang-Landau [18,19] and Metropolis algorithms), as well as obtaining the thermodynamic properties of the model in the core of Husimi cacti [20]. A fully occupied lattice corresponds to the limit of infinite chemical potential, for which only the HDL and an isotropic, disordered phase (corresponding to what is identified as the gas phase in previous studies of the ALG) are expected, since the LDL phase becomes metastable

already for small values of the chemical potential [14,15,17]. Indeed, we find a single transition between the isotropic and the ordered HDL phase, whose loci, nature, and universality class will be addressed in detail in the following.

The remainder of this paper is organized as follows. In Sec. II we detail the model. Simulation methods and results are presented in Sec. III. In Sec. IV mean-field solutions of the model on Husimi cacti are devised. Finally, in Sec. V, we discuss our conclusions and perspectives for future work. Some details on the Husimi lattice solutions are presented in the Appendix.

II. MODEL

We consider the ALG introduced in Ref. [9] in its symmetric version [14]. The model was proposed in the context of waterlike anomalies; despite its simplicity, it captures some features of liquid water, such as density [9,14] and diffusion [10] anomalies. The model is defined on a triangular lattice (coordination number $z = 6$) in which each site can be either empty or occupied by a molecule. Each molecule has six arms, four of which are bonding arms, while the other two are nonbonding ("inert"). In the symmetric version [14], all the bonding arms interact in the same manner, there being no distinction between proton donors and receptors. The inert arms do not interact and assume diametrically opposed positions, giving rise to three orientational states, η_i with $i = 1, 2$ or 3. In this work we adopt a different notation from that of Refs. [9] and [14]. We denote the generators of the triangular lattice by $\hat{e}_1$, $\hat{e}_2$, and $\hat{e}_3$, with

$$\hat{e}_1 = \boldsymbol{i}, \tag{1}$$

$$\hat{e}_2 = +\frac{1}{2}\boldsymbol{i} + \frac{\sqrt{3}}{2}\boldsymbol{j}, \tag{2}$$

and

$$\hat{e}_3 = -\frac{1}{2}\boldsymbol{i} + \frac{\sqrt{3}}{2}\boldsymbol{j}. \tag{3}$$

We use the same set of vectors to label the orientational states. Consider, for example, state 1, with bonding arms along $\pm\hat{e}_2$ and $\pm\hat{e}_3$. As illustrated in Fig. 1, we associate the vector $\boldsymbol{\eta}_1 = \hat{e}_1$ with state 1, $\boldsymbol{\eta}_2 = \hat{e}_2$ with state 2 and $\boldsymbol{\eta}_3 = \hat{e}_3$ with state 3. (Thus $\boldsymbol{\eta}$ points along one of the *nonbonding* directions.)

In the ALG, interactions are restricted to nearest-neighbor (NN) pairs, so that the separations $\boldsymbol{r}_i - \boldsymbol{r}_j$ between interacting pairs again fall in the set $\{\pm\hat{e}_j\}$. A particle at site k in state $\boldsymbol{\eta}_i$ has no interaction with its neighbors at sites $\boldsymbol{r}_k \pm \hat{e}_i$ since it has no bonding arms pointing toward these sites. On the other hand, for $i \neq j$ we have $|\hat{e}_i \cdot \hat{e}_j| = 1/2$. Thus the interaction between a pair of particles at sites i and j, separated by $\boldsymbol{r}$ (a unit vector in the set $\{\pm\hat{e}_i, i = 1, 2, 3\}$), can be written so:

$$u_{ij} = -\gamma\left(\frac{4}{3}\right)^2[1 - (\boldsymbol{\eta}_i \cdot \boldsymbol{r})^2][1 - (\boldsymbol{\eta}_j \cdot \boldsymbol{r})^2], \tag{4}$$

where $-\gamma$ denotes the energy associated with a NN particle pair with bonding arms pointed toward each other. Using this,
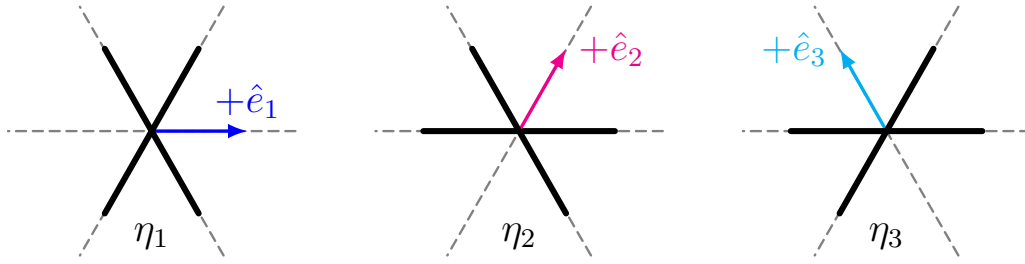
FIG. 1. Definition of orientational states $\eta_1 \equiv \hat{e}_1$, $\eta_2 \equiv \hat{e}_2$, and $\eta_3 \equiv \hat{e}_3$, respectively. The thick black lines represent bonding arms, dashed gray lines represent directions on the triangular lattice, and the arrows indicate the generators of triangular lattice.

the energy of the ALG model may be written:

$$\mathcal{H}(\boldsymbol{\eta}, \boldsymbol{r}) = \sum_{\langle i,j \rangle} \sigma_i \sigma_j [\varepsilon + u_{ij}], \qquad (5)$$

where the summation $\langle i, j \rangle$ runs over pairs of nearest neighbors, the $\sigma_i = 0, 1$ are occupation variables, and $\varepsilon > 0$ represents an orientation-independent repulsive NN interaction. In the present work, we consider full occupancy ($\sigma_i = 1, \forall i$), so that the parameter ε is meaningless and γ is the only remaining parameter in the Hamiltonian. Therefore, from here on we measure energy in units of γ, and define a dimensionless temperature $\tau = k_B T / \gamma$. We remark that when comparing our results with those in the literature for the full model [14,17], one should keep in mind that in these papers the particular case $\gamma/\varepsilon = 2$ was considered, and the parameter ε was used to define the reduced temperature and chemical potential. Thus, in these studies the reduced variables are twice those used here.

At full occupancy, each particle interacts with four of its six neighbors if all particles have the same orientational state (see Fig. 2). Any configuration such that one or more pairs of nearest neighbors have distinct states must have a higher energy. Thus the ground state is threefold degenerate, with energy per particle (in units of γ), $e = -2$. By contrast, the mean energy per particle in a configuration in which each orientation is chosen at random, independently, is $e_{\text{random}} = -4/3$. Since the gain in entropy per site is $\Delta s/k_B = \ln 3$, a crude estimate for the critical temperature is $\tau_c \approx 2/(3 \ln 3) \simeq 0.6$.
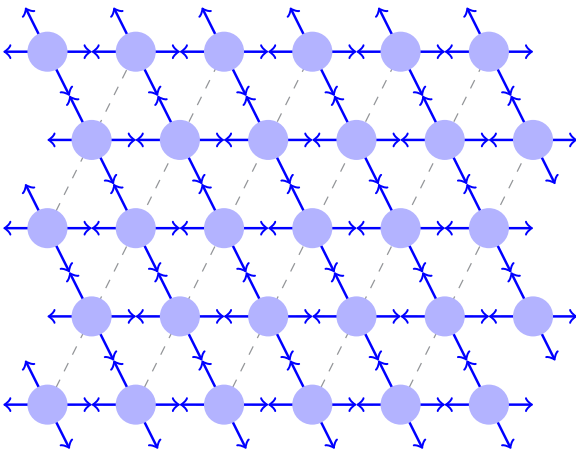

FIG. 2. A ground-state configuration of the fully occupied lattice; all molecules are in the same state.

The model studied here corresponds to the limit $\mu \to \infty$ of the full model, and at low temperatures it will be in the HDL phase. Varying the temperature, we expect to observe a transition from the low-temperature ordered phase, with a majority of particles in one of the orientational states, to a high-temperature disordered one, with equal populations among the three states. This isotropic phase corresponds to the gas phase in the general model. As noted in the Introduction, continuous gas-HDL phase transitions have already been observed in simulations of the nonsymmetric two-dimensional [10] and three-dimensional [12,13,16] ALG models, while a discontinuous transition was found in the mean-field approach for the symmetric model considered here [17]. In the 2D case [10,17], the transition is observed for reduced chemical potentials $\bar{\mu} \equiv \mu/\gamma \gtrsim 1$. Szortika *et al.* [10] proposed an order parameter

$$\theta = \frac{3}{2} \left[\frac{\max(n_1, n_2, n_3)}{N} - \frac{1}{3} \right], \qquad (6)$$

where n_i is the number of particles in state i and N is the total number of particles. Evidently, $\theta = 1$ when all particles are in the same state, and $\theta = 0$ for equally populated states.

In view of the orientation-dependent interaction and the orientationally ordered ground state, we can interpret the transition as one between nematic and isotropic phases. Analysis of such a transition [21] suggests an alternative definition of the order parameter,

$$Q = \frac{1}{N} \sqrt{n_1^2 + n_2^2 + n_3^2 - n_1 n_2 - n_1 n_3 - n_2 n_3}. \qquad (7)$$

Of central interest is the nature of the order-disorder transition in the model at full occupancy. (In principle, we would expect this also to describe the transition at large, but finite μ.) Since the ground state is threefold degenerate, it is tempting to suppose that the transition falls in the three-state Potts class. While this may in fact be the case, we note that the energy, Eq. (5), does not have the symmetry of the Potts model, that is, it is not invariant under permutations among the states. (The ground state is permutation invariant, trivially, but due to the orientational dependence of the interactions, an arbitrary configuration is not.) A similar situation seems to happen in the nematic transition of rigid rods on the triangular lattice [22]. Simulations suggest that the universality class of this transition is also in the three-state Potts model universality class.

In light of the above considerations, we regard it as an open question whether the model belongs to the three-state

Potts universality class. The simulation results reported below provide some insight on this issue.

III. MONTE CARLO SIMULATIONS

A. Simulation details

We performed extensive MC simulations of the symmetric ALG model [14] using both Wang-Landau (WL) simulations [18,19] for triangular lattices with lateral sizes $24 \leqslant L \leqslant 72$, and Metropolis simulations [23] for larger systems. The simulations are performed at full occupancy ($N = L^2$). The WL algorithm is an entropic sampling method, designed to estimate $\Omega(E)$, the number of configurations with energy E. Starting from $\Omega(E) = 1$, $\forall E$, the estimates for Ω are gradually refined in a series of iterations. Each iteration generates a sequence of configurations as described below. An energy histogram, $H[E]$, records the number of configurations having energy E. These simulations use a random initial configuration $\Gamma = \{\eta_i\}$ with energy $E(\Gamma)$. To generate a candidate for the next configuration in the sequence (Γ_{new}), a site i is chosen at random and its state is altered ($\eta_i \to \eta_i'$), generating configuration Γ'. This is accepted as Γ_{new} with probability

$$p[\Gamma \to \Gamma'] = \min \left\{ 1, \frac{\Omega[E(\Gamma')]}{\Omega[E(\Gamma)]} \right\}. \quad (8)$$

With complementary probability, the current configuration Γ is taken as the new configuration. The histogram and logarithm of the number of states are updated so: $H[E(\Gamma_{\text{new}})] \to H[E(\Gamma_{\text{new}})] + 1$ and $\ln \Omega[E(\Gamma_{\text{new}})] \to \ln \Omega[E(\Gamma_{\text{new}})] + \ln f$. The parameter f, known as the modification factor, is set to e, the base of natural logarithms, on the first iteration. A sequence of configurations is generated by repeating this procedure, until the histogram is *flat*, i.e., there is no E such that $H(E)$ is less than (or greater than) $X\%$ of the mean value of the histogram over all energies. Following the usual practice, we use $X = 20\%$, that is, the 80% flatness criterion.

Once the flatness criterion is satisfied, the current iteration ends and a new one is started with the histogram set to zero, but with the $\Omega[E]$ carried forward from the preceding iteration. The new iteration proceeds as before except for a smaller modification factor, taken as the square root of the previous value (i.e., $\ln f \to \ln f /2$). The usual procedure is to end the simulation once $\ln f < 10^{-8}$ or equivalently after 27 iterations.

As is evident from Eq. (8), WL sampling is a kind of Metropolis importance sampling with target probability distribution $P(\Gamma) \propto 1/\Omega[E(\Gamma)]$ in place of the usual Boltzmann distribution, $P(\Gamma) \propto \exp[-\beta E(\Gamma)]$. Thus if iterations extended arbitrarily long and there were no sampling noise, the estimates for the $\Omega(E)$ would converge to their true values. For further details about the convergence (or lack thereof) of WL sampling, see Ref. [24] and references therein.

Recent studies [25] show that it is not necessary to use all 27 iterations of WL sampling. As the modification factor is barely greater than unity, estimates for the $\Omega(E)$ are not significantly modified in the final few iterations. We used 27 iterations for system sizes $L \leqslant 32$, 22 for $32 < L < 72$, and 20 for $L = 72$.

Using the estimates for the $\Omega(E)$, the canonical average of a given thermodynamic observable $\mathcal{O}(E)$ at temperature T can be computed via

$$\langle \mathcal{O} \rangle \equiv \frac{1}{\mathcal{Z}} \sum_E \overline{\mathcal{O}(E)} \Omega(E) \exp(-\beta E), \quad (9)$$

where $\overline{\mathcal{O}(E)}$ represents the microcanonical average and $\mathcal{Z}$ is the canonical partition function. Microcanonical averages are computed as simple averages of property $\mathcal{O}$ over all configurations with energy E generated in the final iteration of the WL procedure. We compute the canonical average of the energy E and its variance, and of order parameters θ and Q and their second through fourth moments.

Although WL sampling yields useful results for systems with $L \leqslant 90$, it is not effective for larger systems. (The time to achieve a flat histogram becomes excessive.) We therefore use standard Metropolis sampling [23] for system sizes $L = 128$ and $L = 256$. In these studies, we use 10^6 MCS for equilibration followed by 2×10^6 MCS to generate data. In both simulation methods, we perform an average over 60 independent realizations, starting from randomly generated initial configurations.

In this section we report simulation results for the model at full occupation. The critical temperature τ_c is obtained via finite-size scaling [26] analysis of the susceptibilities χ_θ,

$$\chi_\theta(\tau) = \frac{L^2}{\tau} [\langle \theta^2 \rangle - \langle \theta \rangle^2], \quad (10)$$

and χ_Q, defined analogously, and of the specific heat c,

$$c(\tau) = \frac{\beta^2}{L^2} [\langle E^2 \rangle - \langle E \rangle^2]. \quad (11)$$

In Eqs. (10) and (11) the terms $\langle \cdots \rangle$ represent canonical averages, L the linear size of the system and τ the temperature. (As already mentioned, our estimates for thermal averages such as θ, χ, and c are averages over 60 independent realizations). The expected finite-size scaling forms for the order parameter, susceptibility, and specific heat are

$$\theta \approx L^{-\beta_\theta/\nu} \mathcal{F}(tL^{1/\nu}), \quad (12)$$

and similarly for Q,

$$\chi \approx L^{\gamma/\nu} \mathcal{X}(tL^{1/\nu}), \quad (13)$$

and

$$c \approx c_0 + L^{\alpha/\nu} \mathcal{C}(tL^{1/\nu}), \quad (14)$$

where β, γ, and α are critical exponents as usually defined, and $t \equiv (\tau - \tau_c)/\tau_c$ is the reduced temperature. Additionally we determined Binder's fourth-order cumulant of the order parameters [27],

$$U_{4,\theta}(T) = 1 - \frac{\langle \theta^4 \rangle}{3 \langle \theta^2 \rangle^2}. \quad (15)$$

$U_{4,Q}$ is defined analogously. At the critical point, U_4 tends to a universal value, characteristic of the universality class, system shape, and boundary conditions employed [28].
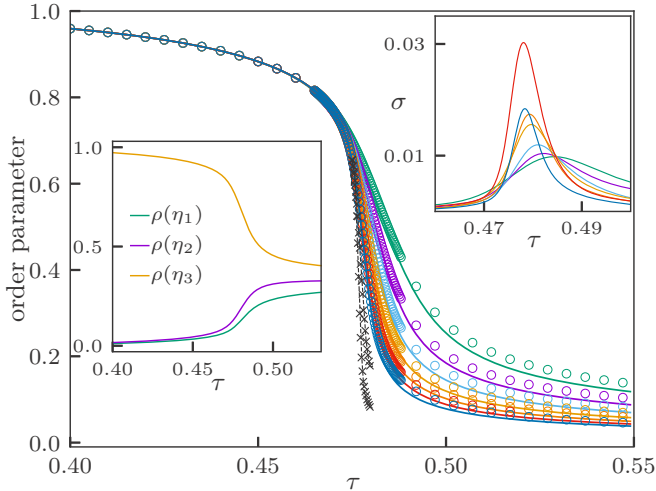
FIG. 3. Order parameters θ and Q versus temperature for system sizes (upper to lower) $L = 24$, 32, 40, 48, 56, 64, 72, 128, and 256. Solid lines and empty circles represent, respectively, θ and Q obtained via the WL algorithm. Black crosses represent results for θ obtained via Metropolis sampling ($L = 128$ and 256); dashed lines represent polynomial fits to the data. Lower inset: Particle fractions ρ in the majority (upper), minority (lower), and intermediate states for $L = 32$. Upper inset: Relative uncertainties for θ in WL simulations; colors follow the main plot.

B. Determining τ_c

The results for the order parameters θ and Q, plotted in Fig. 3, suggest that a continuous phase transition occurs at some temperature in the interval $0.45 < \tau < 0.5$. The lower inset shows the fraction of particles ρ_i in the majority, minority, and intermediate states, for system size $L = 32$, illustrat-
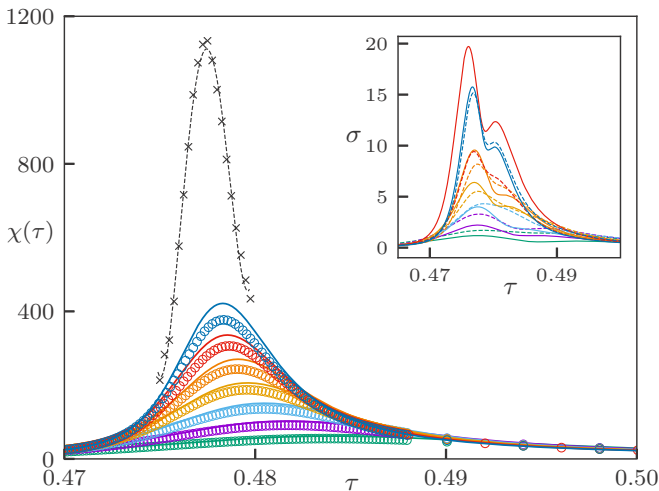

FIG. 4. Susceptibilities versus temperature for system sizes $L = 24$, 32, 40, 48, 56, 64, 72, and 128. Solid lines and empty circles represent, respectively, χ_θ and χ_Q obtained via the WL algorithm. Black crosses represent results for χ_θ obtained via Metropolis simulations ($L = 128$); dashed lines represent a polynomial fit to the data for $L = 128$. (For better visibility, the data for $L = 256$ are not shown.) Inset: Uncertainties in χ_θ (solid lines) and χ_Q (dashed lines).
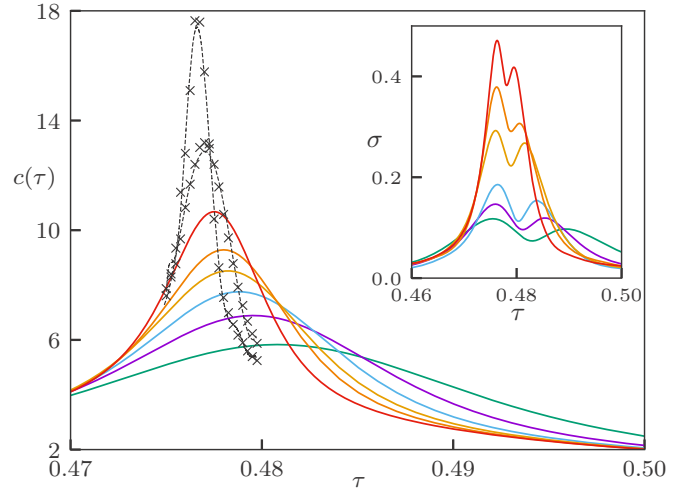

FIG. 5. Specific heat versus temperature for system sizes $L = 24$, 32, 40, 48, 56, 64, 72, 128, and 256. Solid lines represent results from WL simulations and black crosses results obtained via Metropolis sampling for $L = 128$ and 256. Dashed lines represent a polynomial fit to the simulation data. Inset: Uncertainties in c.

ing a continuous variation between ground state (all particles in the same state) and nearly equal populations. Relative uncertainties are plotted in the upper inset. As expected, they are largest in the critical region. In all cases, the relative uncertainty in θ is less than 3%; for system sizes other than $L = 64$, it is <2%.

The susceptibilities χ_θ and χ_Q are plotted in Fig. 4. Although these quantities exhibit similar behaviors, there are slight differences in the critical region; the differences are more evident for larger systems. The discrepancies between the susceptibilities are related to their structures. While Q [see Eq. (7)] takes into account the densities of all three states, θ only involves the majority density [see Eq. (6)]. This may be why the uncertainties (inset Fig. 4) in χ_Q are approximately one-third those in χ_θ. For the sizes shown in Fig. 4, the maximum relative uncertainty in χ_θ is about 6%. The specific heat c, shown in Fig. 5, exhibits behavior consistent with that of the order parameters and susceptibilities. Relative uncertainties in c are smaller than 4% for $48 \leqslant L \leqslant 74$ and smaller than 2% for $L < 48$.

The Binder cumulants of the order parameters are shown in Fig. 6. The crossings of the Binder cumulants for θ and Q provide the estimates $\tau_c^{(Q)} = 0.476(4)$ and $\tau_c^{(\theta)} = 0.476(5)$, respectively.

Using our results for c, χ_θ, χ_Q, and the cumulants, we estimate the critical temperature, τ_c. For c and the χ's, we define a size-dependent *pseudocritical temperature* as the temperature associated with the maximum value. Pseudocritical temperatues for the cumulants are identified as the crossing temperatures of U_4 between: (i) the smallest system size studied, $L = 24$, and the others ($L = 32, \dots, L = 256$), and (ii) the crossing temperatures between a given system size L and the next system size, for example, $L = 24$ with $L = 32$, $L = 32$, with $L = 40$, and so on. The results from the adjacent sizes crossings are represented as U_4'.
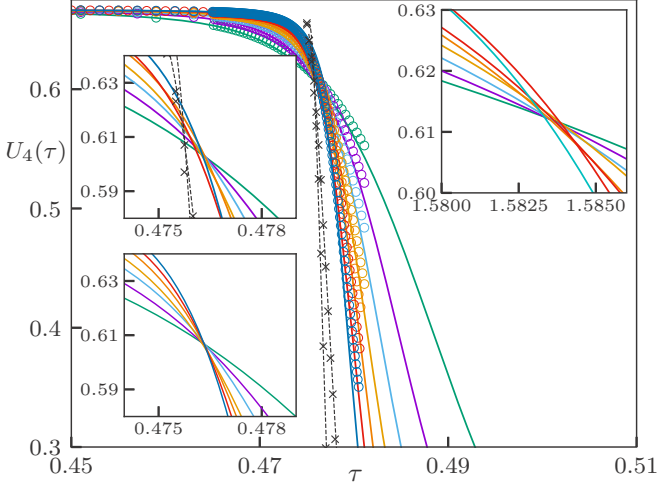
FIG. 6. Binder cumulants $U_{4,\theta}$ (solid lines) and $U_{4,Q}$ (circles) versus temperature for system sizes $L = 24, 32, 40, 48, 56, 64, 72, 128,$ and 256. Crosses: Results for $U_{4,\theta}$ using Metropolis sampling for $L = 128$ and 256. Dashed lines: Sixth-order polynomial fits to the simulation data. Left insets: Detail of the crossing region of $U_{4,\theta}$ (upper) and of $U_{4,Q}$ (lower). Right inset: Cumulant of the three-state Potts model on the triangular lattice for sizes $L = 24, 30, 36, 42, 48, 54, 60, 66,$ and 72.

FIG. 7. Pseudocritical temperatures associated with χ_θ, χ_Q, c, $U_{4,\theta}$, and $U_{4,Q}$, with symbols as indicated, versus $1/L$. Broken lines are fits to the data (quadratic, except for the cumulant data, for which linear fits are very good).

The pseudocritical temperatures are plotted versus $1/L$ in Fig. 7. All six sets of pseudocritical temperatures appear to converge to similar values as $L \to \infty$. Of note is the relative insensitivity to system size of the pseudocritical temperatures derived from cumulant crossings. The crossings between Binder cumulants of two adjacent system sizes for the order parameter θ suffer from large uncertainties for $L \geqslant 64$, affecting the estimate of the pseudocritical temperature. For this reason, we disregard this property in the calculation of the critical temperature.

The resulting estimates for τ_c are listed in Table I. From the six estimates we derive the global estimate $\tau_c = 0.4763(1)$. The global estimate of τ_c was obtained through a weighted average with weights $1/\sigma^2$, where σ represents the uncertainty of each quantity.

C. Critical exponents

Extrapolating the cumulant crossings to infinite size yields two estimates for the critical cumulant: $U_{4,\theta}^* = 0.604(2)$ and $U_{4,Q}^* = 0.606(1)$. Since there can only be one value, a more conservative estimate is $U_4^* = 0.605(2)$. It is of interest to compare this to the critical cumulant of the two-dimensional, three-state Potts model. The best available estimate of the latter, to our knowledge, is Ref. [29] $U_{\text{Potts}}^* = 0.61$. (In Ref. [29],
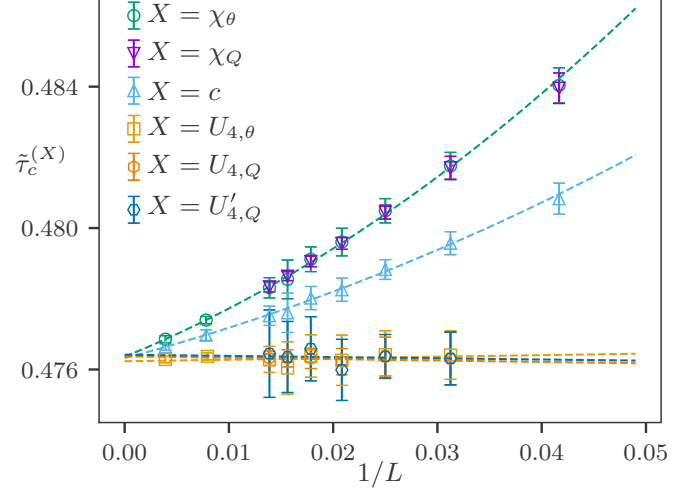
no uncertainty estimate is provided; we may assume it is on the order of 0.01.) In efforts to improve on this estimate we simulated the three-state Potts model on $L \times L$ triangular lattices with periodic boundary conditions. The results for $U_{4,\text{Potts}}$, shown in Fig. 6 (upper-right insert), yield $U_4^* = 0.612(5)$ for the critical cumulant. Although strictly speaking incompatible with our estimate for the associating lattice gas, the two estimates are rather similar, leaving open the possibility of a common universality class for the two models. We also performed a similar study of the three-state Potts model on the square lattice, where we found $U_4^* = 0.6124(8)$, in full agreement with the value for triangular lattice.

We estimate the critical exponent ratios β/ν and γ/ν using fits to the data for θ, Q, and the associated susceptibilities versus system size (see Fig. 8).

From the linear fits shown in Fig. 8(a) and including the effect of the uncertainty in τ_c we obtain $\beta_\theta/\nu = 0.130(3)$ and $\beta_Q/\nu = 0.126(1)$ The inset shows that the residuals are much smaller than the uncertainties, indicating that adding additional terms to the fitting function, in the form of corrections to scaling, would not yield better estimates. The value of this ratio for the two-dimensional, three-state Potts model is [25,30,31] $\beta_{\text{Potts}}/\nu_{\text{Potts}} = 2/15 = 0.1333\ldots$. In the worst case ($\beta_Q$), the discrepancy is about 4%. Linear fits to $\ln \chi_\theta$ and $\ln \chi_Q$ as functions of $\ln L$ [see Fig. 8(b)] yield $\gamma_\theta/\nu = 1.70(2)$ and $\gamma_Q/\nu = 1.73(9)$. Our estimate for γ_θ differs from the value of the three-state Potts model, $\gamma_{\text{Potts}}/\nu_{\text{Potts}} = 26/15 = 1.733\ldots$, by 1.7%. Analysis of the residuals of fits to the

TABLE I. Estimates for the critical temperature. The first six columns (second line) list the estimates for τ_c obtained from analysis of the quantities listed on the first line, while the seventh column contains the global estimate and its uncertainty.

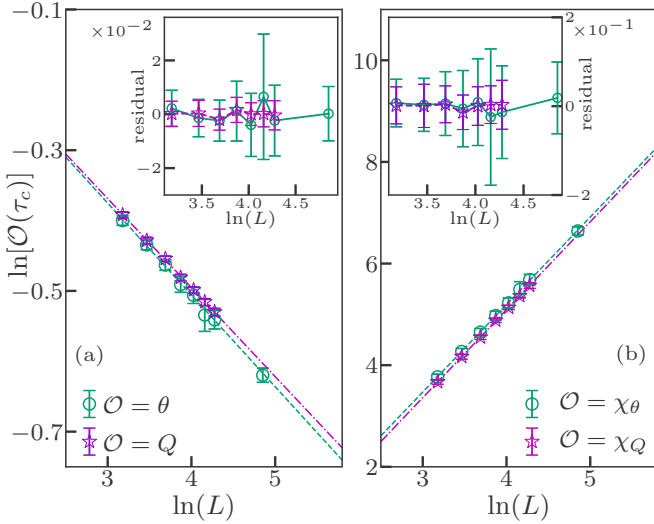| c	χ_θ	χ_Q	$U_{4,\theta}$	$U_{4,Q}$	$U_{4,Q}'$	τ_c
0.47632(1)	0.47636(1)	0.4761(1)	0.47621(2)	0.47637(8)	0.4764(5)	0.4763(1)

FIG. 8. (a) Order parameters θ (Q) versus system size. The circles (stars) represent simulation data; dashed (dot-dashed) lines are least-squares linear fits of the data. Insets show the residuals of the fits. Graphs on the right (b) are analogous plots for the associated susceptibilities.

susceptibilities again indicates that adding further terms to the fitting function is not necessary.

Different from the order parameter and susceptibility, a linear fit to $\ln c$ as a function of $\ln L$ does not yield a good description of the data. We therefore fit the data with $c = aL^{\alpha/\nu} + c_0$ with a, α/ν, and c_0 as adjustable parameters. This form is capable of fitting the simulation data, as can be seen in Fig. 9. The inset shows that the residuals are smaller than the uncertainties and do not exhibit a systematic tendency. A least-squares procedure yields $a = 2.4(6)$, $\alpha/\nu = 0.38(3)$, and $c_0 = -3 \pm 1$. The exponent ratio agrees to within uncertainty with that of the three-state Potts model, $\gamma/\nu_{\text{Potts}} = 0.4$.
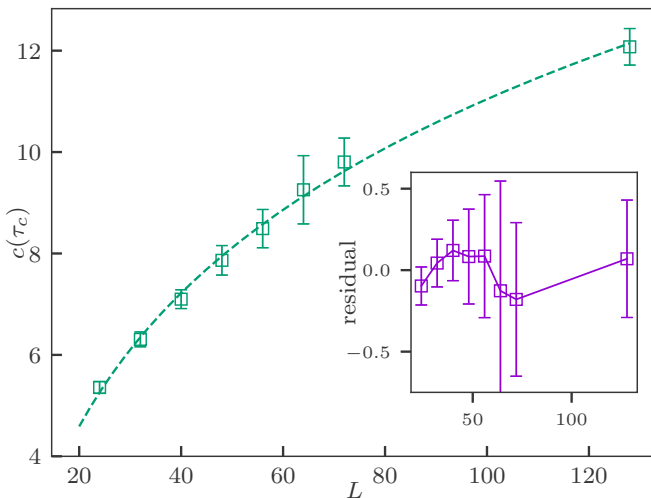

FIG. 9. Specific heat versus system size at critical temperature. Squares: Simulation data with their respective uncertainties. Dashed line: Fit, $c = aL^{\alpha/\nu} + c_0$. The inset shows the residuals, with error bars.
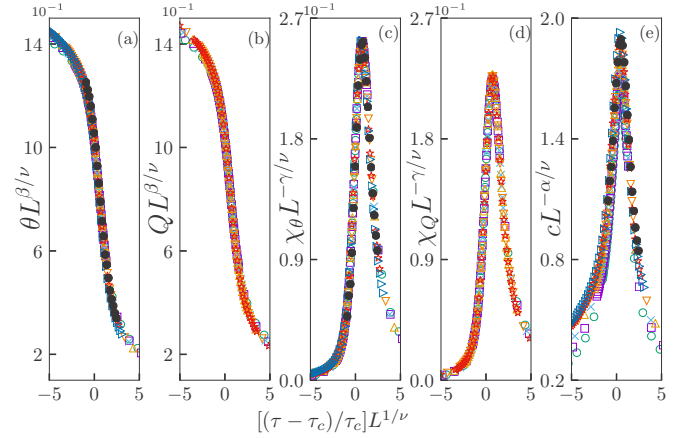

FIG. 10. The panels (a), (b), (c), (d), and (e) exhibit the data collapse for θ, Q, χ_θ, χ_Q, and c, respectively. The symbols $\bigcirc$, $\square$, $\times$, $\triangle$, ∇, $\star$, and $\triangleright$ represent $L = 24, 32, 40, 48, 56, 64, 72$, respectively. Filled black circles ($\bullet$) represent $L = 128$.

Given the scaling relation $\alpha + 2\beta + \gamma = 2$, we have

$$\nu = \frac{2}{\alpha' + 2\beta' + \gamma'}, \qquad (16)$$

where exponents with primes denote the corresponding exponents divided by ν, determined in the finite-size scaling analysis discussed above.

Using the values for β' and γ' obtained using the order parameter θ, Eq. (16) yields $\nu_\theta = 0.85(5)$, while the values associated with order parameter Q furnish $\nu_Q = 0.84(1)$, for an average of $\nu = 0.85(1)$, close to the Potts model value, $\nu_{\text{Potts}} = 5/6 = 0.833\ldots$.

As a further test regarding the universality class, we perform a data collapse using the Potts critical exponents, as shown in Fig. 10. The quantities θ, Q, χ_θ, and χ_Q exhibit a good collapse using these exponents. We observe that the specific heat exhibits the poorest collapse.

The results for the exponents α, β, γ, and ν, as well as for the Binder cumulant strongly suggest that the phase transition studied here belongs to the three-state Potts model universality class. Deviations of the critical exponents from the Potts class values may be due to the flatness criterion, limited sample size, and restricted system sizes.

IV. MEAN-FIELD SOLUTIONS ON HUSIMI LATTICES

A. The Husimi lattice approximations

Generally, mean-field approximations of a particular model correspond also to the solution of this model on a complete graph, with properly rescaled interactions [32]. Since solutions of a model on the core of a Cayley tree (a graph with no loops, in which each node has the same number of neighbors) usually correspond to the Bethe approximation of this model on a regular lattice with the same coordination number as the tree, Baxter suggested that these treelike lattices be called *Bethe lattices* [32]. Additional correlations are taken into account considering *Husimi trees*, built with clusters (polygons or polyhedrons) rather than single sites, so that short closed paths are present. Analysis of a model on the core of a Husimi tree yields its behavior on a *Husimi lattice* [20].
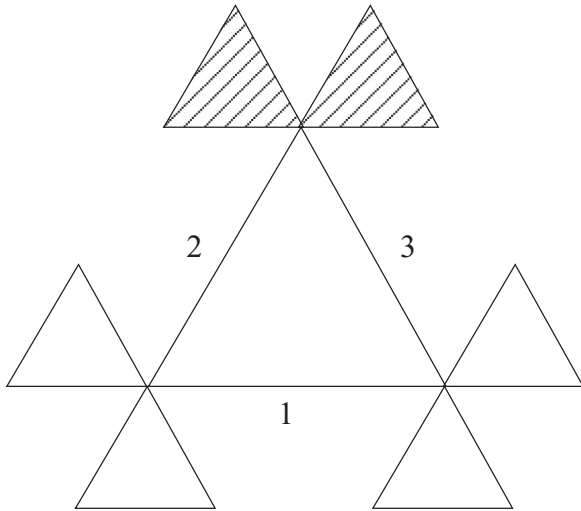
FIG. 11. Six-coordinated Husimi tree built with triangles. Two generations of triangles are shown. The numbers indicate the three directions of lattice edges, as defined in Fig. 1. The hatched triangles should be removed to define a subtree.

We study the ALG model on such treelike lattices, focusing in the limit in which each site is occupied by a molecule. Although we could begin with the six-coordinated Bethe lattice, one readily verifies that the ground state of the model on this lattice, without any closed paths, is highly degenerate. The thermodynamic behavior of the model on the Bethe lattice is qualitatively distinct from that found on the triangular lattice: There is no ordered phase. It is interesting to observe that for the three-state Potts model the Bethe lattice solution already captures the phase transition, although it is found to be discontinuous [33,34]. This is at variance with what is known about its behavior on two-dimensional lattices, where the transition is continuous [30]. For three-dimensional lattices, however, it is found to be discontinuous [30]. We therefore study the model, in the full-occupancy limit, on a Husimi lattice built with triangles, in which three triangles meet at each site, as shown in Fig. 11. We also study the model on a more elaborate Husimi lattice built with hexagons composed of six elementary triangles (see Fig. 12). We remark that the latter case, considering finite chemical potentials, was already studied in Ref. [17], but the limit $(1/\mu \to 0)$ of interest here was not analyzed in that work. As explained in Ref. [17], the use of hexagons in contrast to simple triangles as elementary clusters is imperative for capturing the symmetries of the ground states of the three phases of the full model (gas, LDL, and HDL) on the Husimi lattice; in the case of full occupancy, however, a tree of triangles (Fig. 11) already captures the symmetries. Details on the solution of the complete model on the hexagonal Husimi lattice can be found in Ref. [17], while those for the Husimi lattice built with elementary triangles are presented in the Appendix.

B. Mean-field results

Similarly to our MC simulations on the triangular lattice, in both triangle- and hexagon-Husimi approximations, two stable phases are found for $1/\mu \to 0$. At high temperatures,
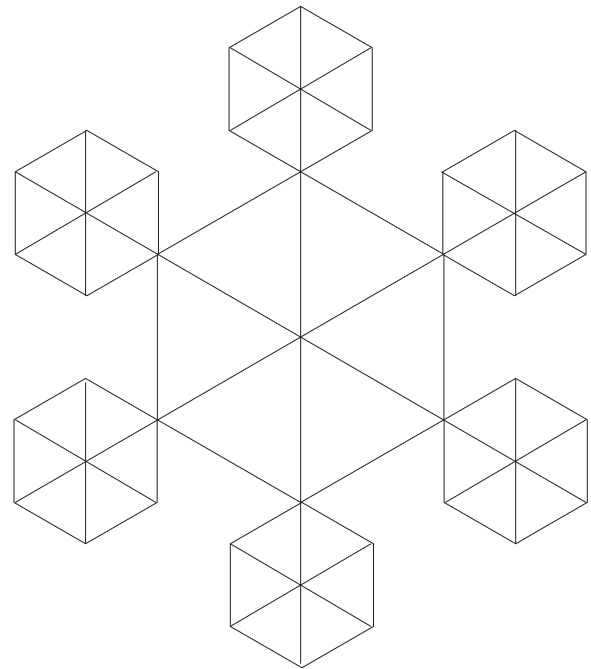

FIG. 12. Husimi tree built with hexagons composed by six triangles. The central hexagon and the six hexagons of the first generation are shown.

only a disordered *isotropic* phase is stable, for which the densities of molecules in the three possible orientations are equal. At low temperatures, three equivalent ordered *nematic* phases are stable, in which the fraction of molecules in one of the three orientations is larger than those in the other two orientations. The stability of the fixed point associated with each phase may be studied using the Jacobian of the recursion relations for the ratios (see the Appendix). This analysis shows that there is a temperature interval in which both fixed points are stable, signalling that the transition between the phases is discontinuous. Thus, to find the coexistence temperature the free energy of the two phases should be equated. It should be remembered that this free energy corresponds to the model on the *core* of the tree; the free energy of the whole tree is dominated by the surface [32,35]. We find a coexistence temperature $\tau_c = 0.51403$ for the triangle tree and $\tau_c = 0.51207$ for the one with hexagons.

The nematic order parameter Q is shown in Fig. 13 as a function of the temperature for both treelike lattices. We note that the transition temperature is reduced, and the jump in the order parameter becomes smaller as we move from the triangle tree to that with hexagons. Also, the temperature interval in which both fixed points are stable becomes narrower (see the Appendix). These results are consistent, as the transition temperature on the triangular lattices estimated from the simulations is still lower and the transition is continuous.

Finally, let us discuss how the transition studied here fits into the general phase diagram of the model for finite chemical potential. The phase diagram of the complete model on the hexagon-Husimi tree is shown in Fig. 14, in the $\tau - \bar{\mu}$ plane. In this diagram we see that the gas-HDL coexistence line, as well as the gas and HDL spinodals, approach vertical asymptotes
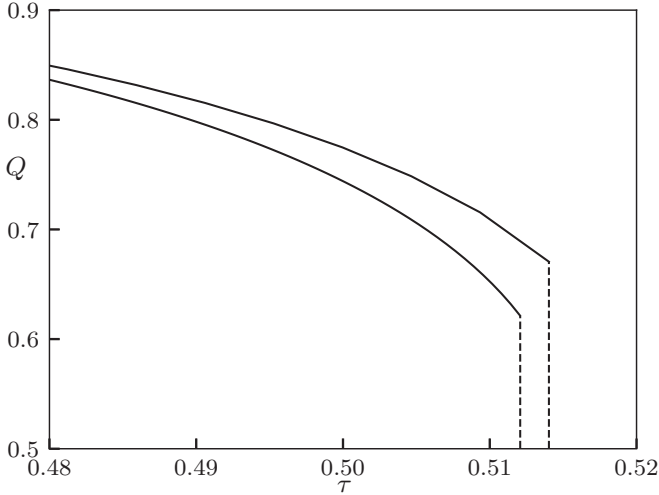
FIG. 13. Nematic order parameter Q as a function of τ close to the coexistence temperature τ_c. The upper curve corresponds to the triangle-Husimi lattice. The lower curve is for the hexagon tree, calculating Q at the central site of the central hexagon, in the limit $1/\mu \to 0$.

and are very close to them already for $\bar{\mu} \gtrsim 10$, whose τ values are very close to those cited above for the solution in the full-occupancy case. Hence, our results for the infinite chemical potential limit correspond to the final point of the coexistence line between the HDL and gas phases. For finite $\bar{\mu}$ the coexisting phases differ in the order parameter Q and in the particle density ρ; the density is lower and Q vanishes in the gas phase. In the full-occupancy limit we consider here, Q still vanishes in the gas phase and is finite in the HDL phase, but $\rho = 1$ in both phases.
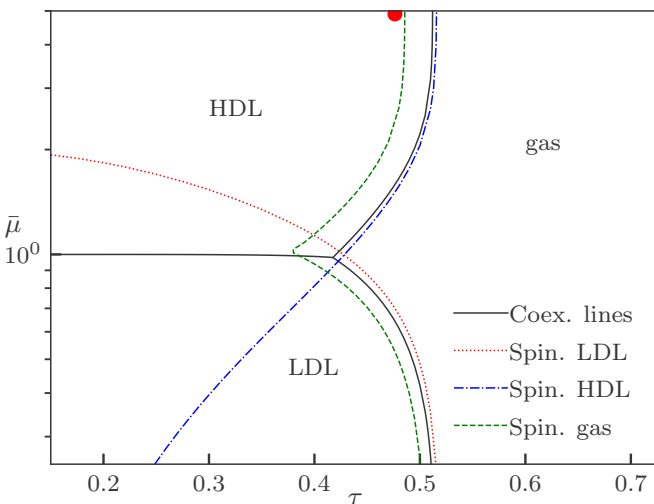

FIG. 14. Phase diagram on the hexagon-Husimi tree for finite chemical potential in the $\bar{\mu}–\tau$ plane. The three phases (HDL, LDL, and gas) are separated by coexistence lines (full lines in graph), which meet at a triple point. Spinodal lines of the phases are also shown. The red circle represents the critical temperature obtained via MC simulations.
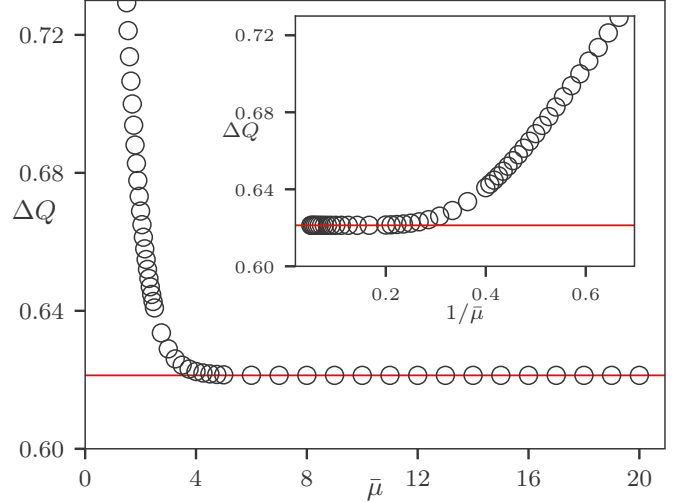

FIG. 15. Discontinuity of the nematic order parameter at the gas-HDL coexistence line as a function of the reduced chemical potential $\bar{\mu}$. The insert shows the same data against $1/\bar{\mu}$.

Figure 15 shows the discontinuity of the nematic order parameter at the gas-HDL coexistence line as a function of the reduced chemical potential $\bar{\mu}$. We note that ΔQ becomes smaller as the chemical potential grows and reaches its minimum value in the limit studied here. We can imagine three possible scenarios for this part of the phase diagram on the triangular lattice. One possibility is that in the limit $1/\mu \to 0$ the gas-HDL coexistence line ends at a critical point. Another would be that the transition becomes continuous already at some finite value of μ, and thus the coexistence line would end at a tricritical point. Finally, the whole transition may be continuous. In this case, if the other transition lines (LDL-HDL and gas-LDL), which meet with the gas-HDL transition line at a triple point on the hexagon tree (see Fig. 14), remain discontinuous, then this point would become a critical end point.

V. CONCLUSIONS

We investigate the isotropic-HDL phase transition of the ALG model [9] in its symmetric version [14] on the triangular lattice in the limit $1/\mu \to 0$ (full occupation) using Monte Carlo simulations and solutions on Husimi lattices. Simulations yield a continuous transition at $\tau_c = 0.4763(1)$. The critical temperature is estimated using finite-size scaling analyses of the order parameters, their susceptibilities, the specific heat, and the fourth-order Binder cumulants. In addition, we derive estimates of U_4^* for the three-state Potts model on the triangular lattice [$U_4^* = 0.612(5)$] and on the square lattice [$U_4^* = 0.6124(8)$], which evidently agree to within uncertainty. Our estimate for U_4 for the three-state Potts model is close to, but more accurate than, one reported previously [$U_4^* = 0.61$] [29]. The critical exponents reported in Sec. IV also support the assertion that the transition belongs to the three-state Potts model universality class.

The mean-field calculations are performed on Husimi trees constructed with triangles and hexagons. Both approaches yield a discontinuous phase transition with coexistence

temperatures somewhat higher than the simulation estimate, viz., $\tau_c = 0.51403$ (triangles) and $\tau_c = 0.51207$ (hexagons). In the second case the difference in relation to the simulation is $\lesssim 7\%$. We note that mean-field calculations for the three-state Potts model in two dimensions also yield discontinuous transitions [36], which may explain the difference found here regarding the nature of the transition in the ALG model.

The complete (mean-field) phase diagram shows a gas-HDL coexistence line which extends from $\bar{\mu} \approx 1$ to $\bar{\mu} \to \infty$, along which a reduction of the discontinuity of the nematic order parameter Q is observed as μ increases. The existence of the discontinuous line gives origin to three possible scenarios that connect the results of simulations and mean field. The first is that at the limit $1/\mu \to \infty$ the line ends in a critical point, the second is a change in the order of transition at a finite chemical potential, and the third raises the possibility of the whole transition be continuous for the triangular lattice. We remark that the ALG model with finite $\bar{\mu}$ is somewhat similar to a diluted three-state Potts system, for which a continuous transition is also observed [37,38]. This suggests that the entire gas-HDL line might be continuous. Another indication of this is the fact that it is continuous in the original 2D ALG model [10], as well as in the 3D version [12,16]. In future work, we intend to perform Wang-Landau sampling, as well as transfer matrix calculations, in order to obtain the complete phase diagram and identify which of the three scenarios mentioned above is correct.

APPENDIX: SOLUTION OF THE MODEL ON HUSIMI TREES

To solve models in the core of treelike lattices, one starts by defining partial partition functions (ppf's) on rooted subtrees, such as the one depicted in Fig. 11 for the lattice built with triangles, for a fixed configuration of the root site. Considering the operation of building a larger subtree connecting smaller ones to a new root polygon, one finds recursion relations for the ppf's. As expected, these partition functions diverge as the recursion relations are iterated indefinitely (this corresponds to the thermodynamic limit), but ratios of these fpp's usually remain finite as the recursion relations are iterated. The stable fixed points attained iterating the recursion relations for the ratios correspond to the thermodynamic limit. The behavior on the complete tree may be found connecting subtrees to a central polygon. Expected values of densities at this central polygon may then be calculated, and may be seen as approximations to the results on the triangular lattice.

In order to solve the model on the Husimi tree built with triangles (see Fig. 11), we have to define nine ppf's $g_{i,\eta}$ of rooted subtrees, where the first index assumes the values 1, 2, or 3 of the direction of the edge opposite to the root site of the triangle. On the subtree obtained removing the hatched triangles in Fig. 11, this index is 1. The second index specifies

the orientation η of the nonbonding arms of the molecule at the root.

The recursion relations are obtained by considering the operation of building a subtree with an additional generation $(M + 1)$ by connecting two pairs of subtrees (with M generations each) to the vertices which are opposite to the root vertex of the new root triangle. We call j_i the orientation of the molecule placed on the vertex opposite to the edge of orientation i of the root triangle. The ppf's of a subtree with $M + 1$ generations are thus obtained through the recursion relations:

$$g_{1,j_1}^{(M+1)} = \sum_{j_2=1}^{3} \sum_{j_3=1}^{3} W_{\{j_1,j_2,j_3\}} g_{1,j_2}^{(M)} g_{1,j_3}^{(M)} g_{2,j_3}^{(M)} g_{3,j_2}^{(M)}, \quad \text{(A1a)}$$

$$g_{2,j_2}^{(M+1)} = \sum_{j_3=1}^{3} \sum_{j_1=1}^{3} W_{\{j_1,j_2,j_3\}} g_{2,j_3}^{(M)} g_{2,j_1}^{(M)} g_{3,j_1}^{(M)} g_{1,j_3}^{(M)}, \quad \text{(A1b)}$$

$$g_{3,j_3}^{(M+1)} = \sum_{j_1=1}^{3} \sum_{j_2=1}^{3} W_{\{j_1,j_2,j_3\}} g_{3,j_1}^{(M)} g_{3,j_2}^{(M)} g_{1,j_2}^{(M)} g_{2,j_1}^{(M)}. \quad \text{(A1c)}$$

The function $W_{\{j_1,j_2,j_3\}}$ is the statistical weight associated to the edges of the root triangle, defined as $W = \exp[2n_b(j_1, j_2, j_3)/\tau]$, where n_b is the number of edges of the triangle with no nonbonding arms on them and τ is the temperature. Thus:

$$n_b(j_1, j_2, j_3) = n_{b,1}(j_2, j_3) + n_{b,2}(j_3, j_1) + n_{b,3}(j_1, j_2)$$
$$= \delta_{j_2,1}\delta_{j_3,1} + \delta_{j_3,2}\delta_{j_1,2} + \delta_{j_1,3}\delta_{j_2,3}, \quad \text{(A2)}$$

where $\delta_{i,j}$ is the Kronecker δ. In this expression $n_{b,i}$ stands for the number of edges in direction i with a bond on them, assuming the values 0 or 1, so that, as expected, $n_b \in [0, 3]$. Thus, the system of nine recursion relations [Eqs. (A1)] allows us to obtain the ppf's of subtrees with an arbitrary number of generations of triangles and, most importantly, the thermodynamic limit (when $M \to \infty$). The ratios of ppf's are defined as

$$R_{i,j} = \frac{g_{i,j}}{g_{i,1} + g_{i,2} + g_{i,3}}, \quad \text{(A3)}$$

which converge to finite values in the thermodynamic limit; six of them are independent, since $\sum_j R_{i,j} = 1$. Therefore, the thermodynamic behavior of the model will be determined by the stable fixed points of the recursion relations for the ratios $R_{i,j}$, which are obtained from Eqs. (A1).

We find fixed points with two different symmetries. In the isotropic fixed point the values of the nine ratios, represented as a 3×3 matrix, are

$$\mathbf{R}_{\text{iso}}^* = \begin{bmatrix} x & (1-x)/2 & (1-x)/2 \\ (1-x)/2 & x & (1-x)/2 \\ (1-x)/2 & (1-x)/2 & x \end{bmatrix}, \quad \text{(A4)}$$

where the parameter x is a function of the temperature τ, whose exact expression can be easily found with the help of an algebra software but is too long to be presented here. The

three nematic fixed points are

$$\mathbf{R}^*_{\text{nem},1} = \begin{bmatrix} x_1 & (1-x_1)/2 & (1-x_1)/2 \\ x_2 & x_3 & 1-x_2-x_3 \\ x_2 & 1-x_2-x_3 & x_3 \end{bmatrix}, \quad (A5)$$

$$\mathbf{R}^*_{\text{nem},2} = \begin{bmatrix} x_3 & x_2 & 1-x_2-x_3 \\ (1-x_1)/2 & x_1 & (1-x_1)/2 \\ 1-x_2-x_3 & x_2 & x_3 \end{bmatrix}, \quad (A6)$$

$$\mathbf{R}^*_{\text{nem},3} = \begin{bmatrix} x_3 & 1-x_2-x_3 & x_2 \\ 1-x_2-x_3 & x_3 & x_2 \\ (1-x_1)/2 & (1-x_1)/2 & x_1 \end{bmatrix}. \quad (A7)$$

Again the parameters x_i, with $i = 1, 2, 3$, are functions of the temperature. We note that the isotropic fixed point is stable at high enough temperatures, while at lower temperatures one of the nematic fixed points is reached. In the isotropic phase the orientation of the nonbonding arms of the molecules has no preferred direction, while in the nematic phase one of the three directions is more probable than the other two. As expected for a discontinuous transition, the isotropic and nematic fixed points are both stable in an interval of temperatures around the coexistence temperature. The region of stability of a given fixed point may be found from the largest eigenvalue of the Jacobian of the recursion relations for the ratios:

$$J_{i,j} = \left(\frac{\partial R'_i}{\partial R_j} \right)_{R^*}, \quad (A8)$$

where R'_i and R_i denotes the ratios in generations $M+1$ and M, respectively, and the derivative is calculated at the fixed point whose stability is being considered. We find that the isotropic fixed point is stable for $\tau \geqslant 0.47299$, while the nematic ones for $\tau \leqslant 0.51970$. Hence, for $\tau \in [0.47299, 0.51970]$ both fixed points are stable, so that the isotropic and nematic phases coexist in this temperature interval. This signals a discontinuous transition between the phases and, then, the coexistence temperature can be determined as the one at which the free energy in the bulk of the tree is equal for both phases.

Following the ansatz proposed by Gujrati [35], we assume that the contribution to the free energy per triangle is different for triangles located at the surface of the tree (ϕ_s) and the ones in the bulk (ϕ_b). In a tree with M generations of triangles, the number of triangles in the bulk is $N_b = 1 + 6 + 6 \times 4 + \cdots + 6 \times 4^{M-2}$, while the number of triangles on the surface is $N_s = 4 \times 4^{M-1}$. Therefore, if φ_M is the free energy of a tree with M generations of triangles, then we find that $\varphi_{M+1} - 4\varphi_M = 3\phi_b$, and since $\varphi_M = -k_B T \ln Y_M$, we have that:

$$\phi_b = -\frac{1}{3} k_B T \ln \frac{Y_{M+1}}{Y_M^4}, \quad (A9)$$

where Y_M is the partition function on the whole tree, which can be obtained by connecting six subtrees to the central triangle. This procedure leads to:

$$Y_M = \sum_{j_1, j_2, j_3 = 1}^{3} W_{\{j_1, j_2, j_3\}} g_{1,j_2}^{(M)} g_{1,j_3}^{(M)} g_{2,j_1}^{(M)} g_{2,j_3}^{(M)} g_{3,j_1}^{(M)} g_{3,j_2}^{(M)}. \quad (A10)$$

In the thermodynamic limit $M \to \infty$, using the recursion relations [Eqs. (A1)], the ratios [Eqs. (A3)] at the fixed points, and this expression for the partition function [Eq. (A10)], the bulk

free energy per triangle may be obtained through Eq. (A9). This yields the coexistence temperature $\tau_c = 0.51403$. Therefore, we indeed have a *discontinuous* transition between the isotropic and nematic phases in the solution of the model on this Husimi lattice.

To further confirm this, we calculate the order parameter Q as defined in Eq. (7). From the partition function (A10) it is simple to obtain the mean value of the number of molecules with orientation i of nonbonding arms in the central triangle:

$$\langle n_i \rangle^{(M)} = \frac{1}{3Y^{(M)}} \sum_{j_1, j_2, j_3 = 1}^{3} n_i W_{\{j_1, j_2, j_3\}}$$
$$\times g_{1,j_2}^{(M)} g_{1,j_3}^{(M)} g_{2,j_1}^{(M)} g_{2,j_3}^{(M)} g_{3,j_1}^{(M)} g_{3,j_2}^{(M)}, \quad (A11)$$

where this number has been normalized so that $0 \leqslant \langle n_i \rangle \leqslant 1$. If we divide the numerator and the denominator by $\prod_{i=1}^{3}(g_{i,1}^{(M)} g_{i,2}^{(M)} g_{i,3}^{(M)})^2$, then we may express this mean values in terms of the ratios, which in the thermodynamic limit assume their fixed point values. The result is

$$\langle n_i \rangle = \frac{\sum_{j_1, j_2, j_3 = 1}^{3} n_i f(j_1, j_2, j_3, \{R^*\})}{\sum_{j_1, j_2, j_3 = 1}^{3} f(j_1, j_2, j_3, \{R^*\})}, \quad (A12)$$

where

$$f(j_1, j_2, j_3, \{R^*\}) \equiv W_{\{j_1, j_2, j_3\}} R^*_{1,j_2} R^*_{1,j_3} R^*_{2,j_1} R^*_{2,j_3} R^*_{3,j_1} R^*_{3,j_2}. \quad (A13)$$

As expected, in the isotropic phase, one has $\langle n_1 \rangle = \langle n_2 \rangle = \langle n_3 \rangle$, so that the order parameter is $Q_{\text{gas}} = 0$. On the other hand, in the nematic HDL phase we find a nonvanishing Q_{HDL}, whose variation with the temperature near the coexistence is displayed in Fig. 13. At the coexistence point the discontinuity in Q is $\Delta Q = 0.67056$.

We performed similar calculations for the tree built with hexagons (shown in Fig. 12), which are actually a particular case of the ones presented in Ref. [17], when all lattice sites are occupied by molecules. For brevity, we will not detail the calculations here, and present the main results only. Since the tree in this case is built with larger clusters, hexagons with one central site and six sites at the border, it is expected that such a calculation should lead to results which are closer to those on the triangular lattice. Again, we find a discontinuous transition, at a somewhat lower temperature, $\tau_c = 0.51207$. The discontinuity in the nematic order parameter at the coexistence is $\Delta Q = 0.6216$, and for $\tau \in [0.48569, 0.51575]$ both fixed points are stable. In this case, since there are effectively four sites per hexagon on the treelike lattice (6/2 at the hexagon's border and the central one), there are more than one way to define the order parameter at the central hexagon. One could, for example, consider just the central *site* or a mean value of the order parameter over all sites of the central *hexagon*. We have done both calculations and found out that these values are quite close. The deviation is maximum at the coexistence temperature and the relative difference is about 0.25% there.

[1] M. Chaplin, Water structure and science, http://www1.lsbu.ac.uk/water/water_structure_science.html.

[2] G. M. bell and D. A. Lavis, Two-dimensional bonded lattice fluids I. Interstitial model, J. Phys. A: Gen. Phys. **3**, 427 (1970).

[3] G. M. Bell and D. A. Lavis, Two-dimensional bonded lattice fluids. II. Orientable molecule model, J. Phys. A: Gen. Phys. **3**, 568 (1970).

[4] D. A. Lavis, The steam-water-ice system: A two-dimensional bonded lattice model. The first-order approximation, J. Phys. C **6**, 1530 (1973).

[5] C. E. Fiore, M. M. Szortyka, M. C. Barbosa, and V. B. Henriques, Liquid polymorphism, order-disorder transitions and anomalous behavior: A Monte Carlo study of the Bell-Lavis model for water, J. Chem. Phys. **131**, 164506 (2009).

[6] Marco Aurelio Alves Barbosa and V. B. Henriques, Frustration and anomalous behavior in the Bell-Lavis model of liquid water, Phys. Rev. E **77**, 051204 (2008).

[7] P. Bruscolini, A. Pelizzola, and L. Casetti, Comment on "Novel Phase Behavior in a Two-Dimensional Network-Forming Lattice Fluid," Phys. Rev. Lett. **88**, 089601 (2002).

[8] M. Šimėnas, A. Ibenskas, and E. E. Tornau, Phase transition properties of the Bell-Lavis model, Phys. Rev. E **90**, 042124 (2014).

[9] V. B. Henriques and M. C. Barbosa, Liquid polymorphism and density anomaly in a lattice gas model, Phys. Rev. E **71**, 031504 (2005).

[10] M. M. Szortyka, V. B. Henriques, M. Girardi, and M. C. Barbosa, Dynamic transitions in a two dimensional associating lattice gas model, J. Chem. Phys. **130**, 184902 (2009).

[11] M. Girardi, A. L. Balladares, V. B. Henriques, and M. C. Barbosa, Liquid polymorphism and density anomaly in a three-dimensional associating lattice gas, J. Chem. Phys. **126**, 064503 (2007).

[12] M. M. Szortyka, M. Girardi, V. B. Henriques, and M. C. Barbosa, Dynamic transitions in a three dimensional associating lattice gas model, J. Chem. Phys. **132**, 134904 (2010).

[13] A. P. Furlan, N. G. Almarza, and M. C. Barbosa, Lattice model for water-solute mixtures, J. Chem. Phys. **145**, 144501 (2016).

[14] A. L. Balladares, V. B. Henriques, and M. C. Barbosa, Liquid polymorphism, density anomaly and H-bond disruption in associating lattice gases, J. Phys.: Condens. Matter **19**, 116105 (2007).

[15] A. P. Furlan, C. E. Fiore, and M. C. Barbosa, Influence of disordered porous media on the anomalous properties of a simple water model, Phys. Rev. E **92**, 032404 (2015).

[16] C. Buzzano, E. De Stefanis, and M. Pretti, Cluster-variation approximation for a network-forming lattice-fluid model, J. Chem. Phys. **129**, 024506 (2008).

[17] T. J. Oliveira, J. F. Stilck, and Marco Aurelio A. Barbosa, Solution of an associating lattice-gas model with density anomaly on a husimi lattice, Phys. Rev. E **82**, 051131 (2010).

[18] F. Wang and D. P. Landau, Efficient, Multiple-Range Random Walk Algorithm to Calculate the Density of States, Phys. Rev. Lett. **86**, 2050 (2001).

[19] F. Wang and D. P. Landau, Determining the density of states for classical statistical models: A random walk algorithm to produce a flat histogram, Phys. Rev. E **64**, 056101 (2001).

[20] K. Husimi, Note on Mayers' theory of cluster integrals, J. Chem. Phys. **18**, 682 (1950).

[21] M. Plischke and B. Bergersen, *Equilibrium Statistical Physics*, 3rd ed. (Worl Scientific, Singapore, 2006).

[22] J. Kundu, R. Rajesh, D. Dhar, and J. F. Stilck, Nematic-disordered phase transition in systems of long rigid rods on two-dimensional lattices, Phys. Rev. E **87**, 032103 (2013).

[23] N. Metropolis, A. W. Rosenbluth, M. N. Rosenbluth, A. H. Teller, and E. Teller, Equation of state calculations by fast computing machines, J. Chem. Phys. **21**, 1087 (1953).

[24] R. Belardinelli, V. Pereyra, R. Dickman, and B. Lourenço, Intrinsic convergence properties of entropic sampling algorithms, J. Stat. Mech. (2014) P07007.

[25] A. A. Caparica, Wang-landau sampling: A criterion for halting the simulations, Phys. Rev. E **89**, 043301 (2014).

[26] M. E. Fisher and M. N. Barber, Scaling Theory for Finite-Size Effects in the Critical Region, Phys. Rev. Lett. **28**, 1516 (1972).

[27] K. Binder, Critical Properties from Monte Carlo Coarse Graining and Renormalization, Phys. Rev. Lett. **47**, 693 (1981).

[28] W. Selke, The critical binder cumulant for isotropic ising models on square and triangular lattices, J. Stat. Mech. (2007) P04008.

[29] T. Tomé and A. Petri, Cumulants of the three-state Potts model and of nonequilibrium models with c_{3v} symmetry, J. Phys. A **35**, 5379 (2002).

[30] F. Y. Wu, The Potts model, Rev. Mod. Phys. **54**, 235 (1982).

[31] T. Nagai, Y. Okamoto, and W. Janke, Crossover scaling in the two-dimensional three-state Potts model, Condens. Matter Phys. **16**, 23605 (2013).

[32] R. J. Baxter, *Exactly Solved Models in Statistical Mechanics* (World Scientific, London, 1985).

[33] F. Peruggi, F. di Liberto, and G. Monroy, J. Phys. A: Math. Gen. **16**, 811 (1983).

[34] F. di Liberto, G. Monroy, and F. Peruggi, The Potts model on Bethe lattices, Z. Phys. B **66**, 379 (1987).

[35] P. D. Gujrati, Bethe or Bethe-Like Lattice Calculations are More Reliable than Conventional Mean-Field Calculations, Phys. Rev. Lett. **74**, 809 (1995).

[36] L. Mittag and M. J. Stephen, Mean-field theory of the many component Potts model, J. Phys. A **7**, L109 (1974).

[37] B. Nienhuis, A. N. Berker, E. K. Riedel, and M. Schick, First- and Second-Order Phase Transitions in Potts Models: Renormalization Group Solutions, Phys. Rev. Lett. **43**, 737 (1979).

[38] X. Qian, Y. Deng, and H. W. J. Blöte, Dilute Potts model in two dimensions, Phys. Rev. E **72**, 056132 (2005).